The Effect of Al^{3+} Additive on the Structural, Optical, and Magnetic Properties of Al–Cd Ferrites Fabricated by Coprecipitation Method

T. Şaşmaz Kuru[a,*], V. Eyüpoğlu[b] and F. Yildiz[c]

[a]Vocational School of Health Services, Radiotherapy Program, Istanbul Okan University, Istanbul, Turkey
[b]Department of Chemistry, ÇankırıKaratekin University, UluyazıCampus, Çankırı, Turkey
[c]Department of Physics, Gebze Institute of Technology, İzmit, Kocaeli, Turkey

(Received October 23, 2017; revised version May 22, 2018; in final form August 10, 2018)

In the present study, Al–Cd ferrites of nominal composition $Al_xCd_{1-x}Fe_2O_4$ (x = 0–0.5) were prepared by coprecipitation method. The effect of Al^{+3} additive on the structural, optical, and magnetic properties of the as-prepared Al–Cd ferrites was investigated. Samples were characterized by X-ray diffraction, scanning electron microscopy, the Fourier transform infrared spectroscopy, UV spectroscopy and vibrating sample magnetometer techniques. The magnetic analysis indicated that all of the samples in different compositions showed ferromagnetic behavior. Along with the X-ray diffraction patterns, the formation of single-phase cubic spinel structure and the lattice parameter were identified in the range of 8.6492–8.6984 Å. Scanning electron microscopy measurements showed that the smallest ferrite nanoparticles were obtained when the stoichiometric composition factor (x) value was 0.4. As an additional characterization, the Fourier transform infrared spectra was investigated, and the characteristic absorption, bands belonging to ferrite nanoparticles were identical around 530 cm^{-1} and 430 cm^{-1}. The tetrahedral and the octahedral complex formation was proved by the observation of higher frequency (ν_1), and lower frequency (ν_2) bands by Fourier transform infrared method, respectively. UV-Vis characterization performed for the determination of E_g values depending on changing Al concentration and found as 2.07–2.24 eV. From the magnetic measurements, all the Al-doped Cd ferrites exhibit S-shaped narrow hysteresis loops revealing soft ferromagnetic nature of the formed ferrites.

DOI: 10.12693/APhysPolA.134.1092

PACS/topics: Al–Cd ferrites, coprecipitation, structural and morphological properties, optical properties, magnetic properties

1. Introduction

Ferrites have been used for many different purposes in science and technology such as communication equipment, electronic devices, magnetic drug delivery, and computers for recent years [1]. Ferrite based materials are known as readily producible, most abundant and cheaper magnetic materials in the scientific literature. Ferrite nanomaterials have attracted a great deal from their electrical properties such as high electrical resistivity and low dielectric loss, magnetic properties, and broad range applications from microwave to radio frequencies [2, 3]. These unique properties can be changed depending on the preparation conditions like the composition, preparation methods, sintering temperature and time [3, 4]. The relationship between electrical and magnetic properties of chemical and structural parameters have not been fully resolved yet. However, the variation of the electrical conduction depending on the temperature is still thought as a reason for this correlation [2]. The concentrations level of ferrous and ferric ions and their dispersion between the tetrahedral and octahedral structures have a significant role in the determination of their magnetic and electrical properties of ferrite nanoparticles [5].

Cadmium-containing ferrite nanoparticles are known as typical spinel structure ferrites. They are usable for different purposes due to their attractive electric, magnetic, and optic properties [6]. However, their physical and chemical properties have not been enough considered by scientists yet, and need to do more research in this field. Al–Cd based ferrites have mixed spinel structure, in which the sites are occupied by Cd^{2+}, and Fe^{3+} ions and B sites were held by Al^{3+} and Fe^{2+} ions in the cubic spinel lattices [7]. Also, good chemical stability, mechanical hardness, low coercivity, and moderate saturation of magnetization properties of cadmium ferrites make them a perfect candidate for applications as soft or flexible magnets, more inferior cost materials at high frequencies [8].

Many of the physical or chemical synthesizing methods have been utilized to produce the nanoferrites. In the form of powdery, thick or thin film ferrites have been prepared by conventional double sintering technique, a coprecipitation method, traditional ceramic method, a sol-gel method, high-temperature solid-state reaction method, etc. [9–13]. The main point to achieve high-performance ferrite synthesis depends on finding a specific technique to incline it giving the compositionally stoichiometric product. In this context, to prepare well-homogenized powder, chemical coprecipitation has been used as a promising method in the present work. This method guarantees the homogeneity of the metal-based

*corresponding author; e-mail: tugba.sasmaz@okan.edu.tr

ionic media in a chemical solution at the initial of the preparation to produce fine particles, while they are precipitating. In addition, the high-density ferrites with fine grain size can synthesized by the coprecipitation method using good precision pH measurement.

In the present study, we investigated how to change lattice constant, grain size, relative density, IR absorption bands, energy band gap, and magnetic properties of spinel-structured ferrite $Al_xCd_{1-x}Fe_2O_4$ ($0.0 \leq x \leq 0.5$) nanoparticles on the addition of different stoichiometric rate of Al into the ferrite mixture. Also, the role of the direct and indirect interactions between cations and anions over the octahedral B-sites in these compounds were illuminated. The prepared materials are characterized by using X-ray diffraction (XRD), Fourier transforms infrared spectra (FTIR), scanning electron microscopy (SEM), and UV techniques. Magnetic properties of the samples have been detected by VSM at room temperature, and the results showed that the ferrites exhibit ferromagnetic behavior with Al substitution.

2. Experimental technique

2.1. Materials

The compounds $Fe(NO_3)_39H_2O$, $Al(NO_3)_39H_2O$, $Cd(NO_3)_24H_2O$ and NaOH, were purchased from Merck, Germany ($> 99.0\%$) and directly used for the synthesis of $Al_xCd_{1-x}Fe_2O_4$ based ferrite nanoparticle samples without further purifications. All aqueous solutions were prepared with deionized water (Milli-Q ultrapure water).

2.2. Synthesis of ferrite nanoparticles

Ferrite nanoparticles were synthesized according to the template of $Al_xCd_{1-x}Fe_2O_4$ with different stoichiometric rates (x = 0, 0.1, 0.2, 0.3, 0.4, 0.5) by the chemical coprecipitation procedure [14]. The aqueous solutions in desired concentrations were prepared by dissolving stoichiometric amounts of $Fe(NO_3)_39H_2O$, $Al(NO_3)_39H_2O$ and $Cd(NO_3)_24H_2O$ in deionized water shown in Table I. The solution was taken into the three-necked reaction flask having 500 ml internal volume and was heated up to 80 °C using a water bath. The solution continuously stirred with a homogenizer to obtain a homogeneous solution. When the temperature of the metal solution was reached to 80 °C, the NaOH solution (2.0 M) was added dropwise to the reaction mixture with a dropping funnel to precipitate the ferrite nanoparticles with controlling pH values and with stirring continuously. The precipitation process was finished by the time the pH value reached up to 11–12. The solid residues were filtered and washed with deionized water to remove the water-soluble impurities, especially NaOH remaining in the precipitate. The resulting precipitate was dried in an oven at 105 °C. After that, the precipitates were sintered in air atmosphere at 800 °C for 8 h with a heating rate of 5 K/min, to obtain the pure spinel ferrite nanoparticles. All steps followed in the preparation process are shown in Fig. 1.

TABLE I

Required salt amounts for solutions to be prepared in 5 ml of pure water.

x [mol]	$Al(NO_3)_39H_2O$ [g]	$Cd(NO_3)_24H_2O$ [g]	$Fe(NO_3)_39H_2O$ [g]
0	0	1.5424	4.04
0.1	0.187565	1.38816	4.04
0.2	0.37513	1.23392	4.04
0.3	0.562695	1.07968	4.04
0.4	0.75026	0.92544	4.04
0.5	0.937825	0.7712	4.04

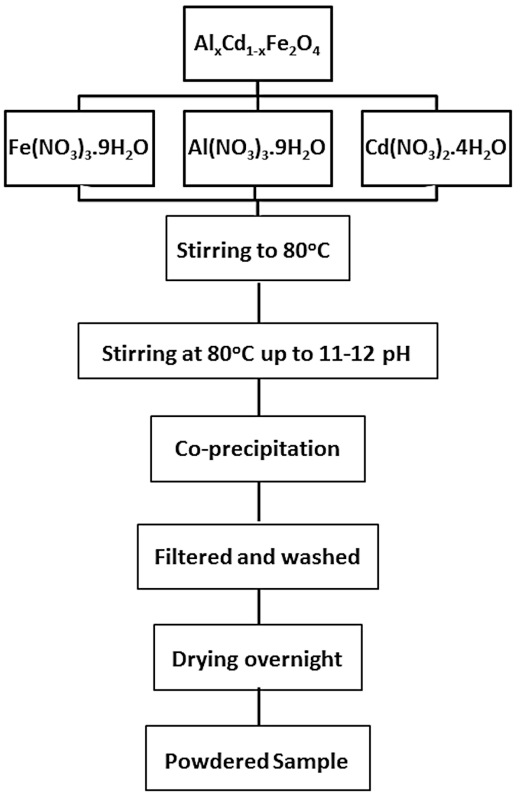

Fig. 1. The synthesis route of ferrite nanoparticle powder.

2.3. Characterization

XRD analysis was performed with X-ray diffractometer (Rigaku D/MAX/2200/PC model device) using Cu K_α radiation ($\lambda = 1.54050$ Å) with 1°/min scanning speed using a grazing angle of 5° in the 2θ range between 10° and 90°. The morphology and microstructures of the composite coating were characterized by a scanning electron microscope (SEM, model JEOL - JSM 6060 LV) at an acceleration voltage of 20 kV.

3. Results and discussion

3.1. The assessment of X-ray diffraction

The XRD patterns of $Al_xCd_{1-x}Fe_2O_4$ ferrite samples are shown in Fig. 2. These patterns were compared with standard JCPDF 00-022-1063. The entire peaks

can be indexed to a cubic spinel structure of $CdFe_2O_4$ with negligible amounts of impurities of CdO and Fe_2O_3 as shown in Fig. 2. The increase of the Al content in $Al_xCd_{1-x}Fe_2O_4$ ferrite affected the formation of the CdO and Fe_2O_3 phases. The crystallinity in the cubic structure of $CdFe_2O_4$ is restored by the addition of Al as a dopant. Maximum peak intensity can be seen at $x = 0.2$, which is confirmed by the increase in the intensity of the peaks as observed by others [15].

Average crystallite sizes of $Al_xCd_{1-x}Fe_2O_4$ samples were calculated by using Scherrer's equation,

$$D = \frac{0.9\lambda}{\beta \cos\theta}, \tag{1}$$

where D — average size of the crystallites, θ glancing angle ($2\theta/2$) and β — full width at half maximum (FWHM) for the sharpest peak (311) [16].

The lattice constants a of the cubic $Al_xCd_{1-x}Fe_2O_4$ cell were calculated using d-spacing and hkl parameters by using the following relation:

$$a = \frac{\lambda \left[h^2 + k^2 + l^2\right]^{\frac{1}{2}}}{2 \sin\theta}, \tag{2}$$

where hkl are the Miller indices. X-ray densities of the sample ($\rho_{\text{X-ray}}$) were calculated using the lattice constant values [17]:

$$\rho_{\text{X-ray}} = \frac{8M}{Na^3}. \tag{3}$$

In Eq. (3), M is the molecular weight of the sample, N is Avogadro's number, and a is lattice constant.

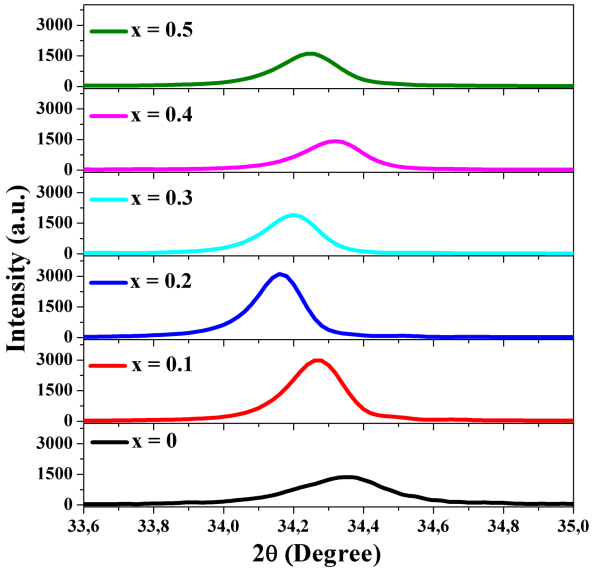

Fig. 2. XRD spectra of $Al_xCd_{1-x}Fe_2O_4$ ferrite nanoparticle.

The extended XRD graph of the most dominant peak (311) of the $Al_xCd_{1-x}Fe_2O_4$ ferrite series is shown in Fig. 3. As can be seen, peak intensity and full width at half maximum (FWHM) were changed by the addition of Al. These two quantities have changed inversely proportional to each other. The effects of x value change on the

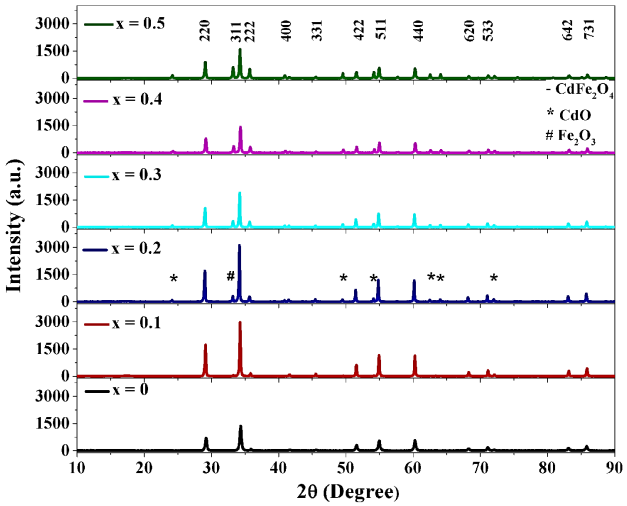

Fig. 3. Extended XRD graph of (311) peak.

TABLE II

Average crystallite size and lattice parameter of $Al_xCd_{1-x}Fe_2O_4$ ferrite

Al content	D [nm]	a_{311} [Å]	$\rho_{\text{X-ray}}$ [g/cm^3]
0.0	28.37	8.6492	5.911
0.1	45.93	8.6735	5.680
0.2	51.69	8.6984	5.466
0.3	45.95	8.6885	5.312
0.4	41.17	8.6590	5.192
0.5	42.16	8.6784	4.980

average crystal sizes are visible. This phenomenon shows that there is an insignificant impurity phase besides the single-phase cubic structure [18]. The obtained average crystallite sizes and lattice parameters have been given in Table II. The average crystallite size varies between 28.37 to 42.16 nm. Also, using Eq. (2), lattice parameters calculated between 8.6492 and 8.6984 Å. As seen in Table II, all the quantities have changed harmoniously within themselves with the changing Al additive.

The effect of Al contents on the variation of average crystallite size has been demonstrated in Fig. 4. This variation is due to the various sites of the unit cell. The increase in the average crystallite size is because Al dopant is rising from 0 to 0.1. While Al contents increased the average crystallite size was decreased. This result may be due to molecular weights or atomic radius of Al^{3+} and Cd^{2+} ions. As the value of x increases from 0 to 0.5, the increased amount of Al cannot provide the decreasing amount of Cd, so it can be considered reasonable to obtain such a result. We can also evaluate this trend in the average crystallite size with another way. This change may result from various sites of the unit cell [19]. The increase in average crystallite size is because the Al^{3+} ions are located in octahedral sites instead of tetrahedral sites. The decrease of the average crystallite size with increasing content of Al^{3+} is due to the compressive stress of Al^{3+} ions [20]. Reference structure cell of the cubic spinel $CdFe_2O_4$ has been shown in the inset of Fig. 4 [21].

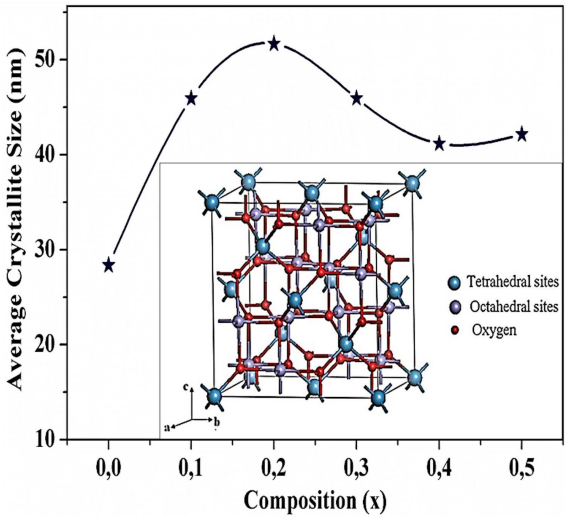

Fig. 4. Variation of crystallite size with the composition for $Al_xCd_{1-x}Fe_2O_4$ ferrite. (Inset: reference structure cell of the cubic spinel $CdFe_2O_4$.

3.2. The assessment of SEM micrographs

The factors affecting the physical and electrical properties of $Al_xCd_{1-x}Fe_2O_4$ based ferrite nanoparticles have been considered to be morphological structure and grain shape determination in different stoichiometric rates (x = 0, 0.1, 0.2, 0.3, 0.4, 0.5) according to related articles [22–24]. Therefore, the micrographs of $Al_xCd_{1-x}Fe_2O_4$ nanoferrite samples were characterized by a scanning electron microscope (SEM, model JEOL - JSM 6060 LV) at an acceleration voltage of 20 kV on changing x values in the range of 0–0.5. The results were shown in Fig. 5. The SEM imaging was performed on the sintered ferrite samples at 800 °C. The valuable change in morphology and grain shape of ferrite samples was observed with the investigation of SEM micrographs. As seen in Fig. 5, the accumulation or aggregation formation among ferrite nanoparticles was observed. Stoichiometrically increase of x values causes to decrease in the stoichiometric rate of Fe atoms in the molecular structure of the ferrite. It was observed from the SEM assessment that the aggregation of the nanoparticles varies depending on the stoichiometric rate of Fe atoms. Some planar or spinal shapes seen on SEM micrographs; especially when x values were 0.2. In the other micrograph, the aggregations among ferrite nanoparticles were random, although their visible shape was powdery. This formation attributed to the mass balance between Cd and Fe atoms. Lower or higher stoichiometric rate of Cd on Fe resulted in smaller nanoparticle formation.

3.3. The assessment of FTIR spectra

Infrared spectroscopy assessment of $Al_xCd_{1-x}Fe_2O_4$ nanoparticles performed to further investigation the structure of the cadmium ferrites doped with different amounts of aluminum. The results of FTIR characterization in the wave number 400–4000 cm^{-1} are shown in

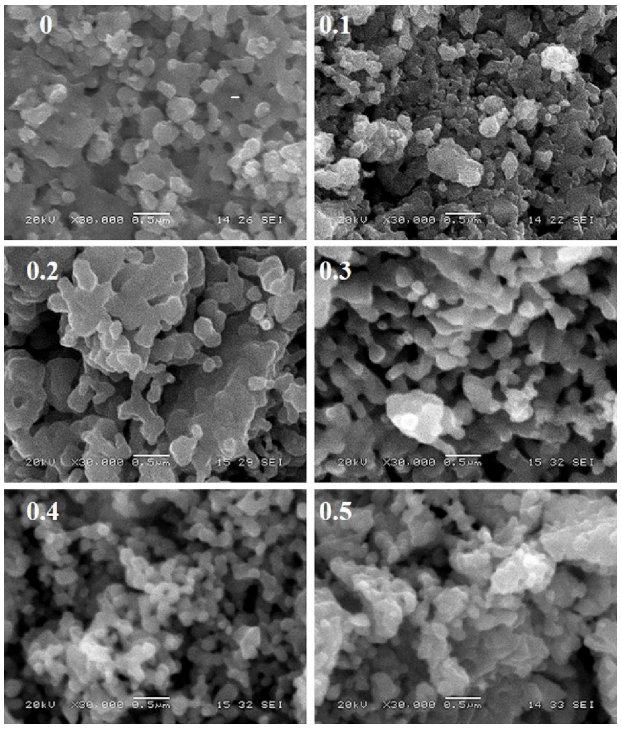

Fig. 5. SEM micrographs of ferrite nanoparticle $Al_xCd_{1-x}Fe_2O_4$ for (a) $x = 0$, (b) $x = 0.1$, (c) $x = 0.2$, (d) $x = 0.3$, (e) $x = 0.4$, and (f) $x = 0.5$.

Fig. 6. There are two absorption bands under 600 cm^{-1}. These IR bands are defined as v_1 and v_2 [25, 26]. The v_1, attributed to the intrinsic stretching vibrations of the metal in the tetrahedral sites, has a higher wave number [22]. v_2, which has less wave number than v_1, is attributed to the intrinsic stretching vibrations in the octahedral sites of the metal [27]. v_1 frequencies are observed around 530 cm^{-1} and v_2 frequencies are observed around 430 cm^{-1}. These results show that the $Al_xCd_{1-x}Fe_2O_4$ nanoparticles have characteristics of spinel ferrites [28]. Peaks that around 1415 cm^{-1} assigned to NO_3 ions, and about 3350 cm^{-1} attributed to hydrogen-bonded O–H groups of water.

3.4. The assessment of optical properties

The UV-vis spectra of $Al_xCd_{1-x}Fe_2O_4$ nanoparticles are shown in Fig. 7 between 200 and 1100 nm regarding percent diffuse reflectance (DR%) and $[\alpha h\nu]^2$ vs. photon energy $h\nu$ graphs were demonstrated in Fig. 8. All samples absorbed light in the range of 300–500 nm. The DR% of the samples are quite high in the range of 600–800 nm. The most senior values in the NIR-infrared region are observed when $x = 0$ and 0.2.

The UV absorption spectrum and band gap energies of the $Al_xCd_{1-x}Fe_2O_4$ nanoparticles was obtained from the reflection spectrum $F(R)$ using the formula Kubelka–Munk formula [29]:

$$F(R) \equiv \alpha = \frac{(1-R)^2}{2R}, \tag{4}$$

where α is the absorption coefficient, and R is the reflectance. The Tauc graphics are obtained from the absorption coefficient α and photon energies $h\nu$. From the slope of Tauc graphs E_g values of the samples are calculated [30].

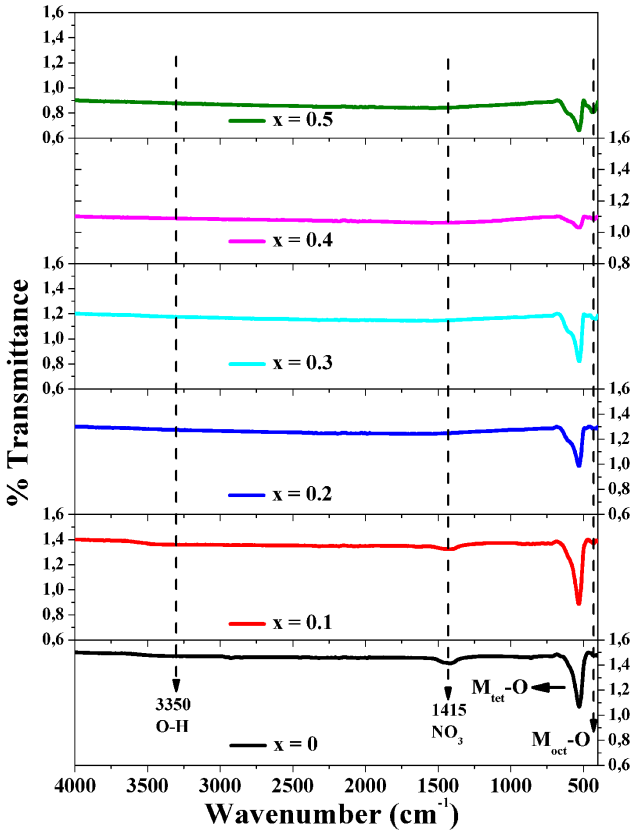

Fig. 6. FTIR spectra of $Al_xCd_{1-x}Fe_2O_4$ ferrite nanoparticles.

The E_g values corresponding to x values are shown in the inset of Fig. 8. E_g values ranged from 2.07 eV to 2.24 eV. These values are compatible with the $CdFe_2O_4$ in the literature [31]. We have not been able to compare the results with Al–Cd ferrite nanoparticles since no such study have been done before. As seen from the Fig. 8, there is not a proportional change between x amounts and E_g values. Therefore, the UV-vis assessments were coherent with the other results.

3.5. The assessment of magnetic properties

Figure 9 represents the room temperature M–H hysteresis loops of $Al_xCd_{1-x}Fe_2O_4$ sample system for varying Al (x) dopant from 0 to 0.5 with a step of 0.1. While there is no Al substitution (for $x = 0$), $CdFe_2O_4$ exhibits a paramagnetic or antiferromagnetic behavior with a zero magnetic moment in the absence of magnetic field. Bulk $CdFe_2O_4$ reported to have a standard spinel structure

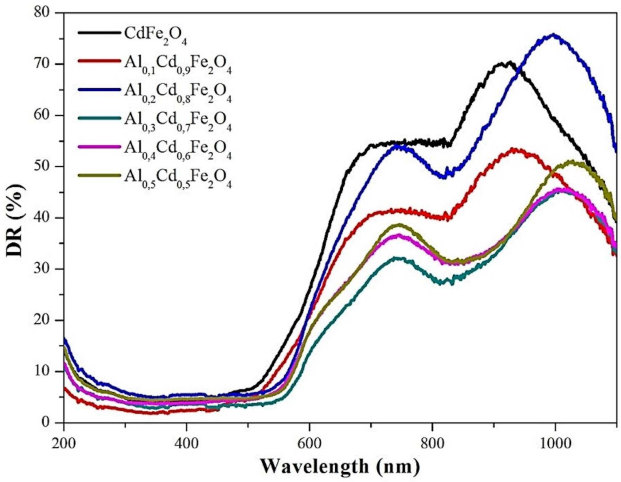

Fig. 7. DR % spectra of $Al_xCd_{1-x}Fe_2O_4$ ferrite nanoparticles.

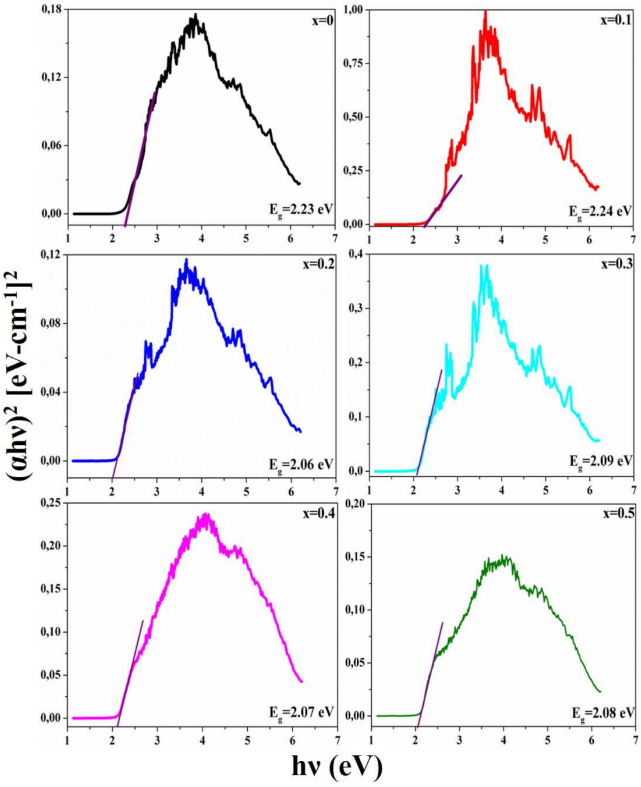

Fig. 8. $[\alpha h\nu]^2$ vs. photon energy $h\nu$ graphs for $Al_xCd_{1-x}Fe_2O_4$. A linear regression to the energy axis gives the E_g.

TABLE III

Variation of magnetic parameters for pure and doped $CdFe_2O_4$ as a function of Al concentration.

Conc. x	M_S [emu/g]	M_r [emu/g]	M_r/M_S	H_C [Oe]
0.1	2.39	0.08	0.03347	40.0
0.2	1.82	0.09	0.04945	125
0.3	0.43	0.03	0.06977	105
0.4	4.91	0.55	0.11202	155
0.5	2.88	0.30	0.10417	150

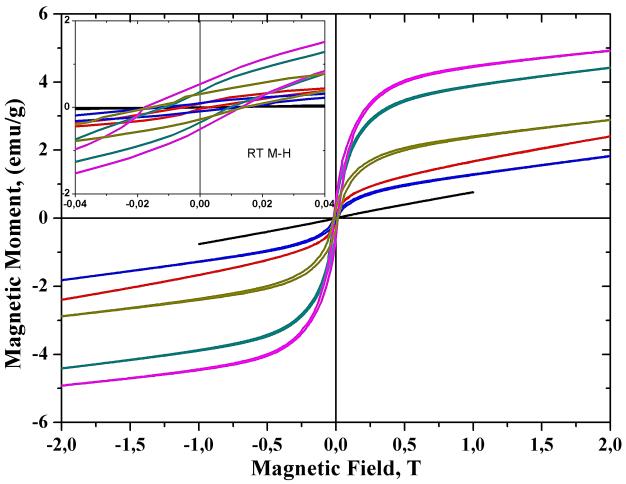

Fig. 9. Magnetic hysteresis loops of $Al_xCd_{1-x}Fe_2O_4$ ferrite system.

and show antiferromagnetic properties [32]. With Al substitution, a non-zero magnetic moment was obtained in the absence of magnetic field for the total dopant concentrations. These assessments can be attributed to the small size and nonmagnetic nature of Al^{2+} ions due to the Néel theory of ferromagnetism [33]. All the Al-doped Cd ferrites exhibit S-shaped narrow hysteresis loops revealing a soft ferromagnetic view of the formed ferrites. Magnetic parameters of our sample system such as saturation magnetization M_S at 20 kOe magnetic field, a remanent magnetization M_r and coercive field H_c values on Al substitution are shown in Table III. The magnitude of these magnetic parameters of the ferrites depends on several factors such as grain growth, exchange interactions between A–B sites of ferrites and dimensions of nanoparticles. In our sample system, magnetic parameters exhibit a non-monotonous behavior on Al dopant concentrations. Nevertheless, most magnificent M_S and H_C values are obtained for $x = 0.4$ dopant concentration. From XRD measurements, the smallest dimensions of our ferrite nanoparticles found for $x = 0.4$ dopant concentration, and that is why greatest M_S and H_C values are obtained for this sample. The phenomenon can explained by the Néel two-sublattice model and the dilution of the magnetizations in A-sites because of non-magnetic Cd^{2+} ions [34, 35]. The reason for the decrease of magnetization beyond $x = 0.4$ is that beyond this limit the magnetization of A-sites are so much diluted that the A–B interaction becomes weaker than the B–B interaction. This mixes up the parallel arrangement of spin magnetic moments on B-site overlay way for skew spins [34].

4. Conclusion

In our study, as a convenient and economical method for the synthesis of Al–Cd based nanoferrites ($Al_xCd_{1-x}Fe_2O_4$), chemical coprecipitation method was followed to prepare the powder samples in different compositions of Al–Cd–Fe because the process has excellent ability to control the particles size and homogeneity of nanoparticles. The produced samples characterized and illuminated in many aspects by XRD, SEM, FTIR, UV-vis, and VSM spectroscopic and imaging techniques. The crystalline structure among ferrite phases was confirmed by XRD analysis, an average crystallite size was calculated as 40 nm. The pattern with certified single-phase cubic spinel structure was with the lattice parameter between 8.6492 and 8.6984 Å. FTIR spectra confirmed the formation of spinel ferrite with the help of two absorption bands at 530 and 430 cm^{-1} due to the stretching vibrations of metal oxide in octahedral sites and tetrahedral sites. Measured band gaps were found between 2.07 eV and 2.24 eV. The magnetic results are not proportional to the x value, but they agree with the structural property results. Greatest M_S and H_C values are obtained for $x = 0.4$ dopant concentration. The M–H hysteresis loops of the $Al_xCd_{1-x}Fe_2O_4$ ferrites were measured at room temperature and there was observed a ferromagnetic behavior with Al substitutions. The samples exhibit the intrinsic magnetic hysteresis loops of the ferromagnetic materials, and the magnetic properties of composites depend on the content of ferrite. So as a conclusion, the prepared and the characterized Al–Cd ferrite nanoparticles can be utilized in various applications that they need to ferromagnetic behavior, with an economic and a sustainable perspective.

Acknowledgments

This work was supported by Sakarya University, Research Project Foundation (FBDTEZ 2016-50-02-10).

References

[1] K.A. Mohammed, A.D. Al-Rawas, A.M. Gismelseed, A. Sellai, H.M. Widatallah, A. Yousif, *Physica B* **407**, 795 (2012).

[2] S. Mahalakshmi, K. Srinivasa Manja, *J. Alloys Comp.* **457**, 522 (2008).

[3] M. Kaiser, *J. Alloys Comp.* **468**, 15 (2009).

[4] A.M. Abo El Ata, S.M. Attia, T.M. Meaz, *Solid State Sci.* **6**, 61 (2004).

[5] E. Ateia, M.A. Ahmed, A.K. El-Aziz, *J. Magn. Magn. Mater.* **311**, 545 (2007).

[6] Munish Gupta, Manik Gupta, Anu, R.K. Mudsainiyan, B.S. Randhawa, *J. Anal. Appl. Pyrolys.* **116**, 75 (2015).

[7] M. Rahimi, M. Eshraghi, P. Kameli, *Ceram. Int.* **40**, 15569 (2014).

[8] Mahmoud Naseri, *J. Magn. Magn. Mater.* **392**, 107 (2015).

[9] R. Sharma, P. Thakur, M. Kumar, N. Thakur, N.S. Negi, P. Sharma, V. Sharma, *J. Alloys Comp.* **684**, 569 (2016).

[10] Ji Bifa, Tian Changan, Zhang Quanzheng, Ji Dongdong, Yang Jie, Xie Jinsong, Si Jingyu, *J. Rare Earths* **34**, 1017 (2016).

[11] Fei Xie, Lijun Jia, Yuanpei Zhao, Jie Li, Tingchuan Zhou, Yulong Liao, Huaiwu Zhang, *J. Alloys Comp.* **695**, 3233 (2017).

[12] M. Mahmoudi, M. Kavanlouei, *J. Magn. Magn. Mater.* **384**, 276 (2015).

[13] K. Sabri, A. Rais, K. Taibi, M. Moreau, B. Ouddane, A. Addou, *Physica B* **501**, 38 (2016).

[14] C.F. Zhang, X.C. Zhong, H.Y. Yu, Z.W. Liu, D.C. Zeng, *Physica B* **404**, 2327 (2009).

[15] N.M. Deraz, M.M. Hessien, *J. Alloys Comp.* **475**, 832 (2009).

[16] M. Tan, Y. Köseoğlu, F. Alan, E. Şentürk, *J. Alloys Comp.* **509**, 9399 (2011).

[17] J. Parashar, V.K. Saxena, Jyoti, D. Bhatnagar, K.B. Sharma, *J. Magn. Magn. Mater.* **394**, 105 (2015).

[18] M.A. Dar, D. Varshney, *J. Magn. Magn. Mater.* **436**, 101 (2017).

[19] P.S. Anil Kumar, J.J. Shrotri, S.D. Kulkami, C.E. Deshpande, S.K. Date, *Mater. Lett.* **27**, 293 (1996).

[20] I. Sadiq, I. Khan, E.V. Rebrov, M. Naeem Ashiq, S. Naseem, M.U. Rana, *J. Alloys Comp.* **570**, 7 (2013).

[21] Y.H. Hou, Y.L. Huang, S.J. Hou, S.C. Ma, Z.W. Liu, Y.F. Ouyang, *J. Magn. Magn. Mater.* **421**, 300 (2017).

[22] T.J. Shinde, A.B. Gadkari, P.N. Vasambekar, *J. Magn. Magn. Mater.* **322**, 2777 (2010).

[23] Q. Li, W. Wang, W. Yongfei, *J. Alloys Comp.* **494**, 315 (2010).

[24] M.N. Ashiq, N. Bibi, M.A. Malana, *J. Alloys Comp.* **490**, 594 (2010).

[25] N. Sharma, P. Aghamkar, S. Kumar, M. Bansal, Anju, R.P. Tondon, *J. Magn. Magn. Mater.* **369**, 162 (2014).

[26] E. Şentürk, Y. Köseoğlu, T. Şaşmaz, F. Alan, M. Tan, *J. Alloys Comp.* **578**, 90 (2013).

[27] Sheenu Jauhar, Sonal Singhal, *Ceram. Int.* **40**, 11845 (2014).

[28] B.K. Labde, Madan C. Sable, N.R. Shamkuwar, *Mater. Lett.* **57**, 1651 (2003).

[29] Abdülhadi Baykala, Sadik Güner, Ayşe Demir, *J. Alloys Comp.* **619**, 5 (2015).

[30] S. Güner, I.A. Auwal, A. Baykal, H. Sözeri, *J. Magn. Magn. Mater.* **416**, 261 (2016).

[31] M. Naseri, *J. Magn. Magn. Mater.* **392**, 107 (2015).

[32] R. Desai, R.V. Mehta, R.V. Upadhyay, A. Gupta, A. Praneet, K.V. Rao, *Bull. Mater. Sci.* **30**, 197 (2007).

[33] L.G. Antoshina, A.N. Goryaga, A.I. Kokorev, *J. Magn. Magn. Mater.* **258**, 516 (2003).

[34] S.S. Bellad, S.C. Watawe, A.M. Shaikh, B.K. Chougule, *Bull. Mater. Sci.* **23**, 83 (2000).

[35] P.N. Vasambekar, C.B. Kolekar, A.S. Vaingankar, *Mater. Chem. Phys.* **60**, 282 (1999).